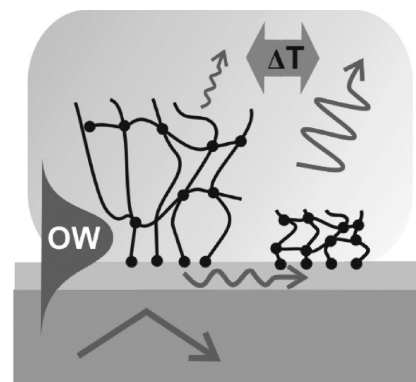


Optical Waveguide-Enhanced Diffraction for Observation of Responsive Hydrogel Nanostructures

Federica Pirani, Nityanand Sharma, Alberto Moreno-Cencerrado, Stefan Fossati, Christian Petri, Emiliano Descrovi, José L. Toca-Herrera, Ulrich Jonas, Jakub Dostalek*

Optical diffraction measurements are reported for in situ observation of swelling and collapsing of responsive hydrogel nanostructures. The optical signal is enhanced by probing the surface carrying periodic arrays of hydrogel nanostructures by resonantly excited optical waveguide modes. UV-nanoimprint lithography is employed for the preparation of the arrays of nanopillars from photo-crosslinked *N*-isopropylacrylamide (pNIPAAm)-based hydrogel that are covalently tethered to a gold surface. The thermo-responsive properties of such pNIPAAm nanopillars that swell in 3D are compared to those of a thin film prepared from the identical material and that is allowed to swell predominantly in 1D. The nanopillars with a diameter of ≈ 100 nm and aspect ratio of 2 swell by a factor of ≈ 6 as determined by optical measurements supported by simulations that are compared to morphological characteristics obtained from atomic force microscopy. Bending of nanopillars above the lower critical solution temperature (LCST), erasure of the topographic structure by drying at temperature below the LCST, and recovery by subsequent swelling below the LCST and drying at temperature above the LCST are observed.



F. Pirani, Dr. N. Sharma, Dr. J. Dostalek, S. Fossati
AIT-Austrian Institute of Technology
Biosensor Technologies
Muthgasse, 11/2, 1190 Vienna, Austria
E-mail: jakub.dostalek@ait.ac.at
F. Pirani
Centre for Space Human Robotics
Istituto Italiano di Tecnologia
Corso Trento, 21, 10129 Torino, Italy
F. Pirani, Prof. E. Descrovi
Dipartimento di Scienza Applicata e Tecnologia
Politecnico di Torino
C.so Duca degli Abruzzi 24, 10129 Torino, Italy
Dr. N. Sharma
Nanyang Technological University
Centre for Biomimetic Sensor Science
School of Materials Science and Engineering
50 Anyang Drive, Singapore 637553, Singapore

A. Moreno-Cencerrado, Prof. J. L. Toca-Herrera
Institute for Biophysics
Department of Nanobiotechnology
University of Natural Resources and Life Sciences Vienna
(BOKU), Muthgasse 11, Vienna 1190, Austria
C. Petri, Prof. U. Jonas
Macromolecular Chemistry
Department Chemistry-Biology
University of Siegen
Adolf Reichwein-Strasse 2, Siegen 57076, Germany
Prof. U. Jonas
Foundation for Research and Technology Hellas (FORTH)
P.O. Box 1527, 71110 Heraklion, Crete, Greece

1. Introduction

Hydrogel micro- and nanostructures have attracted considerable attention in the past decade as they found applications in fields embracing drug delivery,^[1–3] tissue engineering,^[4] and cell biology^[5] as well as other important areas such as analytical technologies,^[6] adhesives,^[7,8] and development of adaptive optical components^[9] and materials.^[10,11] Hydrogel structures tethered to a solid support has been prepared by a range of techniques including photolithography,^[12] e-beam lithography,^[13] nanoimprint lithography (NIL),^[14,15] laser interference lithography (LIL),^[16,17] and colloidal lithography.^[18] Among these, NIL represents an attractive method for its possibility to scaling up and high-throughput.^[19,14,20] A particular class of attractive hydrogel thin film materials are stimuli-responsive systems, which alter their swelling state in response to specific changes of the environment (temperature, pH, etc.).^[21,22] Among responsive polymers, poly(*N*-isopropylacrylamide) (pNIPAAm) holds a prominent stage due to its strong swelling and collapsing that can be triggered by variations of temperature around its lower critical solution temperature (LCST ≈ 32 °C). pNIPAAm have been used in the form of thin films,^[23] composites,^[24] as well as microgels.^[25]

Cryogenic scanning electron microscopy (CRYO-SEM)^[26] was employed for the observation of hydrogel micro- and nanostructures attached to a surface. This method offers powerful means to investigate static morphology and the effects of the chemical composition and crosslinking density of the structure of the hydrogel. Atomic force microscopy (AFM)^[27] allows for in situ observation of hydrogel structures and their responsive properties. Moreover, fluorescence correlation spectroscopy^[28] and dynamic light scattering^[29] provide tools for the characterization of dynamics of polymer chains in hydrogel materials.

Besides these, surface plasmon resonance (SPR) and optical waveguide mode spectroscopy (OWS)^[30] represent convenient means for in situ observation of tethered thin hydrogel films that are allowed to swell and collapse in the direction perpendicular to the surface. Surface plasmon-enhanced diffraction measurements were reported for the observation of thin hydrogel layers that were microstructured by using UV photolithography.^[31] This technique allowed for reference-compensated observations of swelling and collapsing hydrogel layers that occurred predominantly normally to the surface (1D).

This work presents an extension of this approach and it reports on the optical observation of hydrogel nanostructures that can swell and collapse in 3D. It is based on optical waveguide-enhanced diffraction measurements and it takes advantage of strong electromagnetic field intensity enhancement that amplifies the (otherwise extremely weak) diffracted light intensity. With

the aid of an optical model the measured changes in diffraction efficiency are translated to the swelling ratio variations of investigated nanostructures. This method is applied for the investigation of swelling and collapsing of pNIPAAm-based hydrogel nanopillars that are prepared by UV–NIL. The obtained optical results are compared to AFM measurements of the topographic surface structure and unusual behavior (that is not observed for small aspect ratio microstructures) is discussed.

2. Experimental Section

2.1. Polymer Synthesis

A random terpolymer [composed of *N*-isopropylacrylamide, methacrylic acid (MAA), and 4-methacryloyloxy benzophenone in a ratio of 94:5:1] was synthesized by free radical polymerization and thoroughly characterized as described elsewhere.^[32] The *N*-isopropylacrylamide provided thermo-responsive characteristics of the terpolymer, the benzophenone moieties enabled its photo-crosslinking, and the MAA can be used for postsynthetic modification^[33] and it improves the swelling properties. The chemical structure is presented in Figure 1a and the molecular weight of used polymer was 2.49×10^5 g mol⁻¹ and the dispersity was 3.05.

2.2. Layer Preparation

High-refractive index LaSFN9 glass substrates were subsequently coated with 2 nm Cr layer and 47 nm Au film by vacuum thermal evaporation (FL4000, HHV Ltd., UK). Then, SU-8 from Micro Resist Technology GmbH (Germany) that was diluted with SU-8 thinner at ratio of 1:50 was spun onto the Au surface at 5000 rpm for 60 s with 1 s ramping time. The substrates were then dried in a vacuum oven for 2 h at 50 °C. The pNIPAAm polymer was dissolved in ethanol at a concentration of 60 mg mL⁻¹, spun on the SU-8 surface at 2000 rpm for 2 min, and dried overnight at 50 °C in a vacuum oven. The thickness of SU-8 linker layer was ≈ 10 nm and the thickness of dry pNIPAAm film was ≈ 300 nm as measured by SPR and OWS.

2.3. Imprinting of Arrays of pNIPAAm Nanopillars

Dry pNIPAAm film was imprinted by using a polydimethylsiloxane (PDMS, Sylgard 184 from Dow Corning, USA) working stamp. This stamp was prepared from a Si master as described in the Supporting Information. The Si master carried an area of about 1 cm² that was structured by rectangular arrays of nanoholes with a diameter of $D = 90$ nm, depth of 260 nm, and period $\Lambda = 460$ nm. The master structure was casted to Ormo-stamp (from Micro Resist Technology GmbH, Germany) and subsequently transferred to the PDMS. Prepared PDMS working stamp that carried arrays of nanoholes was soaked in ethanol for several minutes. Afterward, the surface of the stamp was dried with a stream of air over several seconds and then brought into conformal contact with the pNIPAAm film. At this point additional 10 μ L of ethanol was dispersed on the top of the stamp

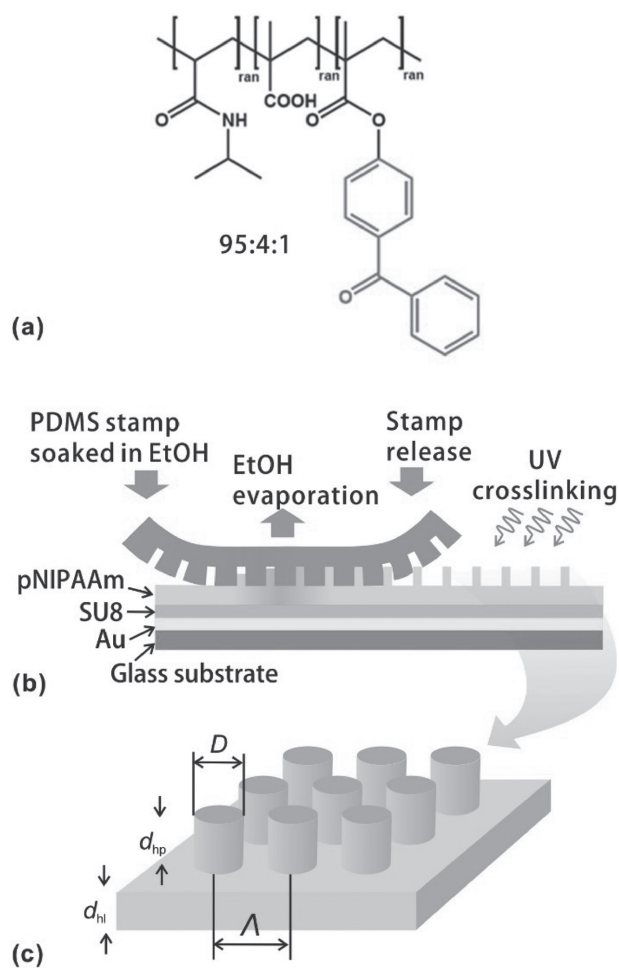


Figure 1. a) Chemical structure of poly(*N*-isopropylacrylamide-co-methacrylic acid-co-4-methacryloyloxy benzophenone) polymer (pNIPAAm). b) Schematics of the imprinting procedure. c) Geometry of pNIPAAm-based nanopillar arrays.

(the opposite side not in contact with the pNIPAAm film). As illustrated in Figure 1b, ethanol diffused through the PDMS to the surface of pNIPAAm layer, partially dissolved the polymer so its upper part becomes fluid and filled the casted nanoholes. The PDMS working stamp was kept in contact with pNIPAAm layer in ambient atmosphere at room temperature for 1 h followed by overnight drying in vacuum. Then, the PDMS working stamp was detached leaving imprinted arrays of nanopillars at the surface of pNIPAAm layer. After storage in vacuum at elevated temperature of 50 °C for several hours, the imprinted pNIPAAm layer was cross-linked by irradiation with UV light at wavelength $\lambda = 365$ nm and dose of 10 J cm^{-2} in a UV chamber Bio-Link 365, Vilber (Germany).

2.4. Atomic Force Microscopy

Ex situ observation of the imprinted pNIPAAm surface was performed in air at room temperature by AFM PicoPlus from Molecular Imaging (USA). The surface was probed in tapping mode by n^+ -silicon cantilevers (PPP-NCHR, Nanosensors, Switzerland)

with a spring constant of 42 N m^{-1} . In situ measurements were performed in water by using a flow cell with temperature control. The polymer surface was then probed by silicon nitride cantilever DNP-S10 from Bruker (USA) with low nominal spring constant of 0.24 N m^{-1} . Prior to its use, the cantilever was cleaned with UV-ozone for 20 min. AFM instrument Nanowizard II from JPK Instruments (Germany) was operated in tapping mode at low forces to prevent sample damage and a scan rate lower than 2 Hz was used.

2.5. Optical Setup

The imprinted pNIPAAm layer was optically probed by OWS that was utilized by using the attenuated total reflection (ATR) method in Kretschmann configuration, see Figure 2. The optical system allowed for the resonant excitation of optical waveguide modes, as described in more detail in our previous work.^[33] Briefly, a laser beam at wavelength of $\lambda = 633$ nm with its intensity modulated by a chopper was coupled to a 90° prism made of LASFN9 glass. A glass substrate with Au film and imprinted pNIPAAm layer was optically matched to the prism base and a flow-cell clamped against its surface. The temperature of water that was flowed through the flow-cell was controlled by a Peltier device, which was connected to a driver LFI3751 from Wavelength Electronics (USA). The whole assembly of prism, glass substrate, and flow cell was mounted on a two-arm coaxial goniometer for the control of the angle of incidence θ (measured outside the prism). Transverse magnetic (TM) and transverse electric (TE) polarization of the incident laser beam was selected by a rotation polarizer and the area illuminated on the surface was of several mm^2 . The laser beam was partially reflected and partially scattered in a series of diffraction orders upon its incidence at the surface with the periodic arrays of pNIPAAm nanopillars. The intensity of reflected light beam R_0 was detected by a photodiode that was connected to a lock-in amplifier 7260 from EG&G (USA). The intensity of -1 st order diffracted beam T_{-1} that transmitted through the flow cell was measured by an identical detector, see Figure 2. The data acquisition and system control was performed by a software tool developed in LabVIEW (National Instruments, USA) and by the software Wasplas (Max Planck Institute for Polymer Research in Mainz, Germany).

2.6. Evaluating of Reflectivity and Diffraction Spectra

Measured angular dependence of reflectivity $R_0(\theta)$ was fitted with a Fresnel-based model implemented in the software Winspall (Max Planck Institute for Polymer Research, Mainz, Germany). In this analysis, refractive indices of Au, Cr, and SU-8 were assumed to be $0.2 + 3.51i$, $3.14 + 3.3i$, and 1.48 , respectively. Thicknesses of these layers were determined by fitting reflectivity spectra $R_0(\theta)$ measured on respective reference samples prior to their coating with pNIPAAm. For the investigation of 1D swelling of pNIPAAm hydrogel film, a “box model” was used (assuming a thickness d_{hl} and homogeneous refractive index over the whole hydrogel layer n_{hl}). In order to capture changes in the geometry of nanopillars from variations in the T_{-1} spectrum, a numerical model based on finite element method was employed. This method was implemented in a diffraction grating solver DiPoG developed at

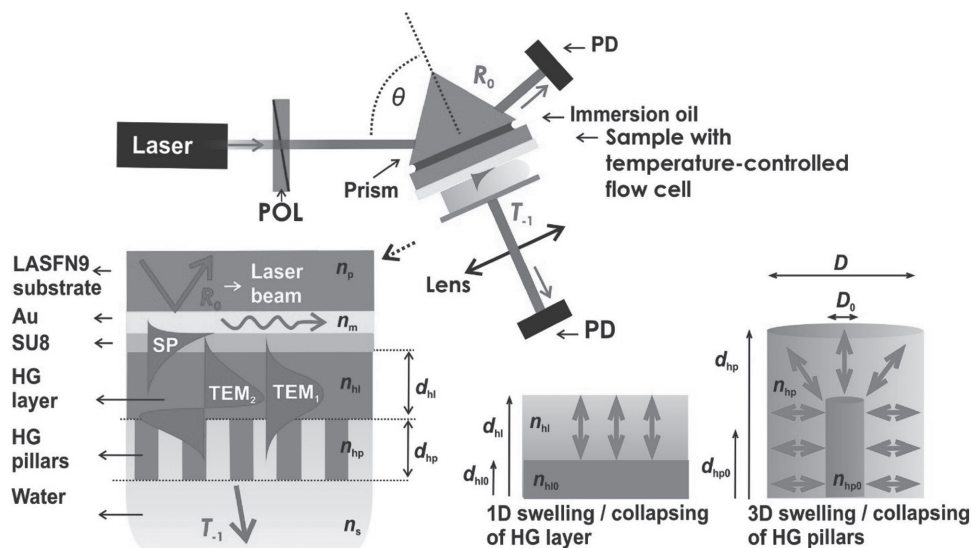


Figure 2. Optical system that was employed for the probing of swelling and collapsing of pNIPAAm-based hydrogel (HG) nanopillar arrays by optical waveguide spectroscopy and optical waveguide-enhanced diffraction. The system utilized a polarizer (POL) and a photodiode (PD), and the sensor surface was probed by surface plasmon (SP) and optical waveguide (TEM) modes travelling along the surface.

the Weierstrass Institute (Germany). The structure was approximated as a linear binary grating with the surface modulated only in lateral direction in the plane of incidence and it was described by width D and height d_{hp} of a dielectric ridge (see Figure 2). The mesh size of the unit cell with a stack of layers and a ridge with the width D and height d_{hp} was adjusted in order to converge simulated reflectivity R_0 and diffraction efficiency T_{-1} .

3. Results and Discussion

First, the topographic structure of freshly imprinted and photo-crosslinked pNIPAAm hydrogel nanopillars before any contact with a swelling solvent was investigated ex situ by AFM. Acquired images in Figure 3a reveal that as-prepared pNIPAAm nanopillar arrays exhibited in air the same period of $\Lambda = 460$ nm as the master structure.

The height of imprinted nanopillars of $d_{hp} \approx 208$ nm was smaller and the diameter $D = 130$ nm (measured at half of the maximum height) was wider compared to the original Si structure ($D = 90$ nm, depth of 260 nm, and period $\Lambda = 460$ nm), which can be ascribed to the multistep replication process. The cross-linked pNIPAAm nanopillar arrays and the underlying pNIPAAm residual layer were allowed to swell in water at temperature $T = 22$ °C. AFM data presented in Figure 3b show that the structure was completely erased after the subsequent drying at the same temperature $T = 22$ °C as the surface flattened. Interestingly, when the surface was swollen again in water at $T = 22$ °C and dried at a higher temperature of $T = 38$ °C after the temperature-induced volume collapse, the array topography of the nanopillars partially recovered on the surface, see Figure 3c. Apparently the topographic erasure of the

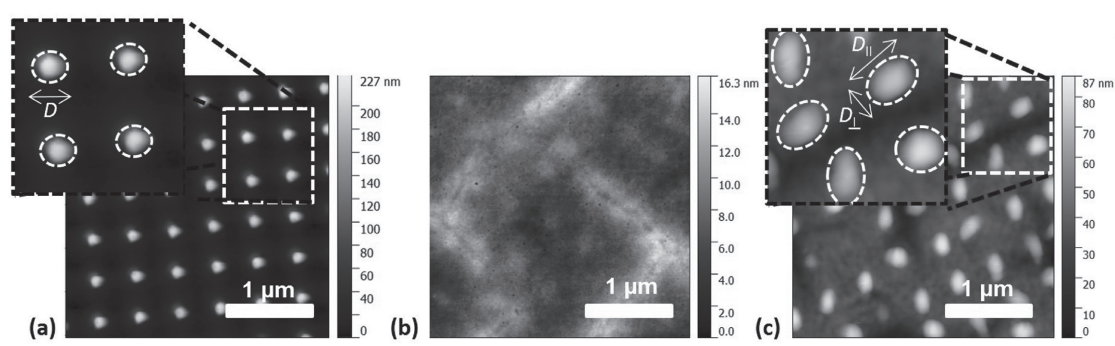


Figure 3. Ex situ AFM observation of a) freshly prepared pNIPAAm nanopillar arrays (before any swelling process) in air compared to the structure that was swollen in water and dried at temperature b) of $T = 22$ °C below the LCST (of around 32 °C) and c) of $T = 38$ °C above the LCST. The scale bar is the same for the three microscopy images.

array features upon drying at low temperature is induced by the strong surface tension of the air–water interface as it passes over the surface structure during water evaporation.^[34] This process leads to the rearrangement of the swollen polymer chains as the surface tension strongly competes (and apparently exceeds) the elastic restoring force of the swollen polymer network. This hypothesis is corroborated by the observation of structure recovery when drying is performed at elevated temperatures above the LCST of 32 °C for the used NIPAAm copolymer.^[32] In this case, the temperature-induced collapse of the pNIPAAm network leads to a substantial increase of the elastic modulus in the hydrogel material. It exceeds the drying forces induced by the water meniscus and thus the nanopillar topography is preserved during water evaporation. The shape of the pillars that were swollen and dried at elevated temperature (Figure 3c) changed compared to that of the freshly prepared arrays (Figure 3a). The nanopillars exhibited decreased height of $d_{\text{hp}} = 76 \pm 6.8$ nm and elongated elliptical footprint with the width in the half maximum of $D_{\parallel} = 288 \pm 12.0$ nm and $D_{\perp} = 205.5 \pm 6.6$ nm along the long and short axis, respectively, after drying at elevated temperature of $T = 38$ °C. The prolonged shape of dry nanopillars indicates that they bend upon the collapse or during the drying step of pNIPAAm hydrogel. Interestingly, volume of swollen and collapsed nanopillars stayed approximately the same ($3.4 \times 10^{-3} \pm 0.5 \times 10^{-3} \mu\text{m}^3$ of pristine nanopillars and $3.55 \times 10^{-3} \pm 0.4 \times 10^{-3} \mu\text{m}^3$ after the swelling and collapsing defined as $\pi D_{\parallel} D_{\perp} d_{\text{hp}}/4$).

Following the AFM characterization, the temperature-induced changes in pNIPAAm nanostructures were optically investigated in situ. The swelling and collapsing of the pNIPAAm layer and arrays of nanopillars were probed by the resonantly excited $\text{TE}_{0,1}$ and $\text{TM}_{1,2}$ waveguide modes travelling along the surface with the hydrogel film. These modes are supported by the hydrogel layer and the propagation of light is confined by the reflective Au surface at the inner interface and by total internal reflection at the outer interface between the hydrogel (exhibiting higher refractive index n_{hl}) and water (exhibiting lower refractive index n_{s}).

Figure 4a,b shows that the resonant excitation of waveguide modes manifests itself as series of characteristic dips in the reflectivity spectrum $R_0(\theta)$. The swollen pNIPAAm-based hydrogel film at low temperature below LCST supports two waveguide modes in transverse magnetic ($\text{TM}_{1,2}$) and transverse electric ($\text{TE}_{0,1}$) polarization. At elevated temperature above the LCST, the layer shrinks and only TE_0 and TM_1 waveguide modes are observed in each polarization. The fitting of measured reflectivity curves with the transfer matrix-based model allowed to determine thickness d_{hl} and refractive index n_{hl} of the pNIPAAm layer at temperatures between $T = 22$ and 50 °C. Results summarized in Figure 4c reveal that the swollen

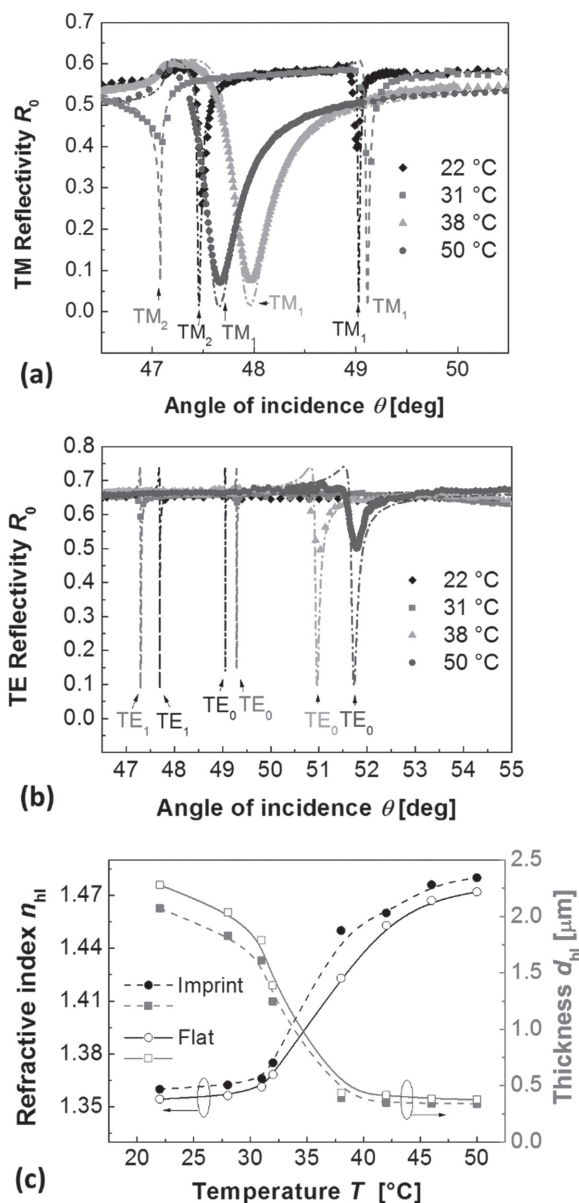


Figure 4. Angular reflectivity $R_0(\theta)$ spectra measured with a) TM and b) TE polarized light for a pNIPAAm hydrogel layer carrying imprinted nanopillar array in its top. The structure was in contact with water at temperatures $T = 22, 31, 38,$ and 50 °C. Symbols indicate measured data and lines show respective fits. c) Determined refractive index n_{hl} and thickness d_{hl} of hydrogel layer with flat and imprinted interface between pNIPAAm and water (lines are guides for the eyes).

pNIPAAm layer at room temperature $T = 22$ °C exhibited a thickness of about $d_{\text{hl}} = 2.3 \mu\text{m}$ and refractive index of $n_{\text{hl}} = 1.356$. When increasing the temperature to NIPAAm LCST = 32 °C, the hydrogel layer abruptly collapsed. When further raising the temperature to $T = 50$ °C, the thickness dropped to $d_{\text{hl}} = 380$ nm and the refractive index increased to $n_{\text{hl}} = 1.47$. The imprinted nanopillar structure in the upper surface of the pNIPAAm layer weakly affected the

spectrum of guided waves in $R_0(\theta)$ and thus the evaluated thickness d_{hl} and refractive index n_{hl} of structured and flat surface are similar. The reason is that imprinting of the nanopillars was accompanied with a transfer of only a small volume fraction (few percent) of the underlying polymer layer into the pillar volume, which led to only a slight decrease in its thickness d_{hl} . The swelling ratio of the hydrogel layer of $SR \approx 6$ at room temperature $T = 22$ °C was determined as the ratio of the thicknesses d_{hl} in swollen and dry states for both imprinted and nonimprinted pNIPAAm layers. This parameter is inversely proportional to the polymer volume fraction Φ_p of the swollen hydrogel material with water, which can be obtained from Maxwell Garnett effective medium theory^[35] as

$$\Phi_p = \frac{n_{\text{hl}}^2 - n_{\text{hlo}}^2}{n_{\text{hl}}^2 + 2n_{\text{hlo}}^2} \bigg/ \frac{n_s^2 - n_{\text{hlo}}^2}{n_s^2 + 2n_{\text{hlo}}^2} \quad (1)$$

where $n_{\text{hlo}} = 1.48$ is the refractive index of the (dry) polymer and n_s is the refractive index of the pure water phase $n_s = 1.332$.^[36] The obtained value for the polymer volume fraction at room temperature of $\Phi_p = 0.17$ is fully consistent with the swelling ratio calculated from the volumetric change (respective layer thicknesses).

The optical observation of swelling and collapsing of pNIPAAm nanopillars was carried out by measuring changes in the intensity of minus first diffraction order T_{-1} . In these measurements, the sample with arrays of pNIPAAm nanopillars was optically matched to the prism in such orientation that the arrays lie in the plane of incidence. The light beam hitting the surface at angles above the critical angle ($\theta > 47^\circ$) was partially reflected back into the prism (R_0 signal) and partially diffracted to -1 st diffraction orders toward the prism (R_{-1}) and toward the water (T_{-1}). It is worth mentioning that for the chosen period $\Lambda = 460$ nm the -1 st diffraction orders travel at angles θ that are close to zero as indicated in Figure 2. Unlike the reflected diffraction order R_{-1} , the intensity of transmitted beam T_{-1} can be easily detected through the transparent flow cell. Figure 5 shows the dependence of the T_{-1} intensity on the angle of incidence θ for (a) TM and (b) TE polarized light beams. These spectra were measured at temperatures between $T = 22$ and 50 °C and they reveal that the overall (relative) T_{-1} intensity does not vary with temperature and it can be ascribed to the background signal. However, a series of strong peaks above this background occurs at angles θ where $TE_{0,1}$ and $TM_{1,2}$ modes are resonantly excited and where the diffraction intensity is amplified. Interestingly, the diffraction of TE polarized light is accompanied with much stronger intensity than that for TM polarization. As presented in Figure 5c, diffraction intensity of the peak associated with the coupling to TE_0 mode increases by a factor up to 30 when changing the temperature from

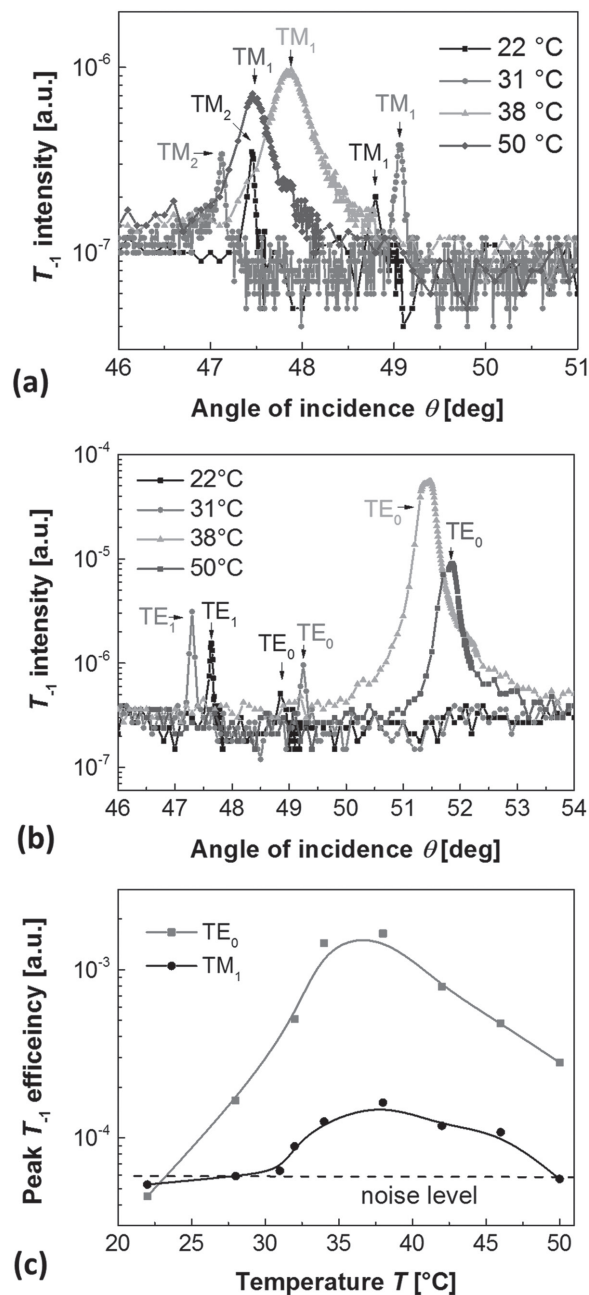


Figure 5. Measured angular spectra of transmitted beam intensity $T_{-1}(\theta)$ for a) TM and b) TE polarization. c) Peak diffraction intensity T_{-1} measured upon the resonant excitation of TE_0 and TM_1 modes (lines are guides for the eyes).

$T = 22$ to 38 °C. This can be attributed to a shrinking of the hydrogel pillars that translates to an increase of their polymer volume fraction Φ_p . These changes lead to higher refractive index of nanopillars n_{hp} and thus enhanced optical contrast of the hydrogel diffraction grating. The magnitude of observed variations in the peak intensity amplified by TM_1 mode is lower than that for TE_0 mode. The reason is that the weaker TM polarized signal is partially masked by background (indicated as a dashed line

in Figure 5c). Therefore, further only TE polarization is used for the investigation of swelling characteristics of prepared pNIPAAm nanopillars. The measured diffraction intensity T_{-1} enhanced by the resonant coupling to TE_0 waveguide modes exhibits its maximum at a temperature of $T \approx 38$ °C. Above this temperature the diffraction intensity gradually decreases and drops again by a factor of about 6 at a temperature of $T = 50$ °C.

The measured dependence of the diffracted beam intensity T_{-1} on temperature was compared with simulations in order to estimate the swelling ratio of the pNIPAAm nanopillars. In the performed simulations, the values for the thickness d_{hl} and refractive index n_{hl} of residual pNIPAAm layer were determined by OWS as described in the previous section. The swelling of nanopillars was assumed to increase their height $h_{hp} = \alpha h_{hp0}$ and diameter $D = \alpha D_0$ by the same factor α (representing a 3D swelling process in contrast to the 1D swelling of the surface-attached hydrogel layer). The refractive index of the hydrogel nanopillar n_{hp} was assumed homogenous and depends on polymer volume fraction Φ_p as follows from effective medium theory^[35]

$$n_{hp} = n_s \sqrt{\frac{n_p^2(1+2\Phi_p) + n_s^2(2-2\Phi_p)}{n_p^2(1-\Phi_p) + n_s^2(2+\Phi_p)}} \quad (2)$$

In order to simplify the numerical analysis, the structure was periodic only in the direction in the plane of incidence (i.e., the nanopillars were represented by ridges with a width D and height h_{hp}). Then the polymer volume fraction of such hydrogel feature can be described by the volume ratio in the swollen and dry states as $\Phi_p = D_0 h_{hp0} / D h_{hp}$. In this equation, values measured for dry nanopillars $D_0 = 130$ nm $h_{hp0} = 208$ nm were used.

In order to translate changes in the optically measured diffraction intensity to the variations of the nanostructure volume, the dependence of T_{-1} diffraction efficiency on the polymer volume content Φ_p was simulated for angles θ where TE_0 and TM_1 modes were resonantly excited. The obtained data plotted in Figure 6a show that the diffraction efficiency T_{-1} amplified by the resonantly excited waveguide modes increases with the polymer volume content of the nanopillars Φ_p which is inversely proportional to the nanopillar volume. Interestingly, the amplification by TE_0 mode translates to T_{-1} intensity that is ≈ 100 -fold higher than that for the TM_1 mode. Such difference in simulated T_{-1} intensity exceeds the experimentally observed values in Figure 5c and it can be explained by the variations in the coupling strength to waveguide modes (see measured data and simulations in Figure 4a,b). The experimentally observed drop in the coupling efficiency can be ascribed to small variations in the thickness of the pNIPAAm layer d_{hl} , which smear resonances in the measured reflectivity [manifested as lower depth of reflectivity dip in $R(\theta)$]. Such smearing is more

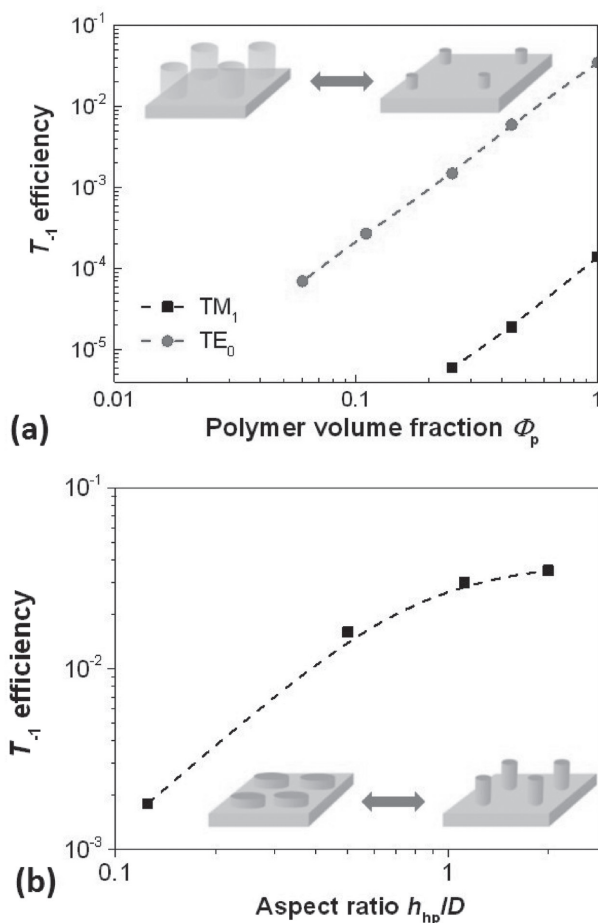


Figure 6. a) Simulated diffraction efficiency T_{-1} , amplified by the resonantly excited TM_1 and TE_0 modes (supported by a swollen hydrogel film) depending on the polymer volume fraction of the nanopillar Φ_p . b) Simulated dependence of T_{-1} diffraction efficiency amplified by TE_1 mode (supported by a collapsed hydrogel film) for varied aspect ratio of the collapsed nanopillar ($n_{hp} = 1.47$). Lines are guides for the eyes.

pronounced for the excitation of TE modes, which exhibit much narrower resonances than TM modes due to the stronger Ohmic losses in the metallic Au film.

The swelling ratio of prepared pNIPAAm nanopillars was estimated by comparing the simulated diffraction efficiency with the measured values. The log–log plot presented in Figure 6a shows a linear decrease of T_{-1} diffraction efficiency with decreasing polymer volume fraction Φ_p . From its slope the change of polymer volume fraction Φ_p by about five times was estimated for the experimentally observed 30-fold change in T_{-1} diffraction efficiency (see Figure 5c). Assuming that the collapsed nanopillars exhibit $\Phi_p = 0.8$ – 0.9 at around 38 °C, the polymer volume fraction of the structure in the swollen state at $T = 22$ °C of $\Phi_p = 0.17$ – 0.2 is predicted based on these results. Indeed, such swelling ratio is similar to that measured for the pNIPAAm layer composed of identical

polymer network attached to a solid support. This observation does not agree with Flory–Rehner theory which suggests that a hydrogel structure which can expand in 3D swells more than a tethered hydrogel film of which swelling is constrained to 1D.^[37] A possible explanation for the observed behavior is that the 3D swelling of nanostructures becomes restricted when their size is comparable to the radius of gyration of the polymer chains.

The effect of nanopillars bending that changed measured T_{-1} diffraction was captured by simulating the optical response for different aspect ratios h_p/D . In these simulations, the volume of a hydrogel feature was kept constant $h_p D = h_{p0} D_0$ and the refractive index was set to $n_{hp} = 1.47$. Data presented in Figure 6b correspond to diffraction on nanopillars in the collapsed state and they confirm that lowering the aspect ratio decreases the diffraction efficiency. This observation is consistent with the measured drop of the diffraction efficiency when raising the temperature from $T = 38$ to 50 °C (see Figure 5c). The measured decrease in aspect ratio of 6 corresponds to the decrease in aspect ratio of ≈ 6 based on simulations in Figure 6b.

In order to verify the OWS data on the swelling and collapsing of imprinted pNIPAAm nanopillars, in situ AFM measurements were carried out in water at temperatures varied from $T = 22$ to 50 °C. At lower temperatures $T < 30$ °C, the imprinted structure was not discernible under the applied AFM conditions and the topography of

the soft pNIPAAm surface exhibited only irregular wavy features (see Figure 7a). Such features can be attributed to a buckling process that is associated with a lateral swelling stress resulting from the covalent surface attachment of the polymer network. This confinement leads to anisotropic swelling of the underlying pNIPAAm layer predominately in the direction perpendicular to the surface. It is worthwhile noting that such buckling behavior was observed for other hydrogel films with thicknesses of several tens of μm and a cross-link density gradient perpendicular to the surface to which they were attached.^[38] Such a cross-link density gradient was also observed by OWS for the herein used pNIPAAm-based films with a swollen thickness of several μm .^[32]

When the temperature approached the LCST of the pNIPAAm network, the imprinted nanopillar structure became apparent in AFM images measured under water. Figure 7b–d illustrates that the height d_{hp} and diameter D of the periodic features decreased with temperature T . The height of contracting pillars of ≈ 45 nm was observed at $T = 31$ °C and it shrunk to ≈ 30 nm at $T = 50$ °C. In addition, Figure 7d clearly indicates that the imprinted pillars bend and lay randomly oriented on the surface at temperatures well above the hydrogel LCST. This is similar to the observations in air (see Figure 3c) but under the present conditions of full immersion in water this effect cannot be due to the surface tension upon the drying and it is rather associated

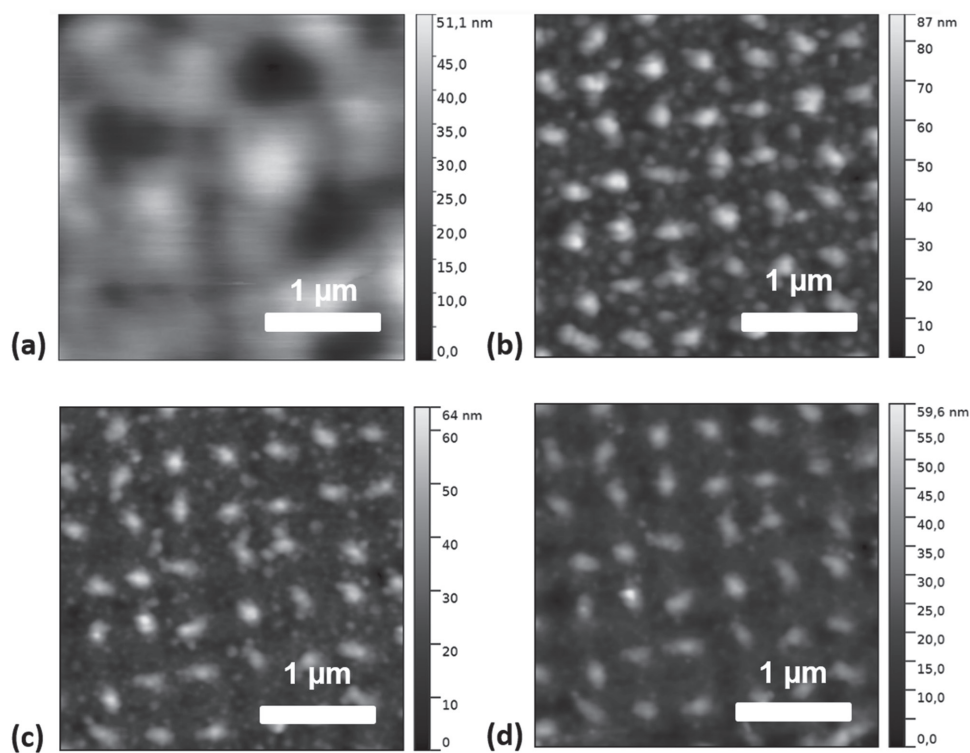


Figure 7. In situ AFM observation in water of pNIPAAm hydrogel nanopillars at temperatures a) $T = 22$ °C (swollen), b) 31 °C (beginning to collapse), c) 38 °C (collapsed and starting to bend), and d) 50 °C (collapsed and bent). The scale bar is the same for the three microscopy images.

with increasing hydrophobic attraction between the pNIPAAm pillars and the underlying pNIPAAm polymer film. The associated hydrophobicity of the pNIPAAm polymer network gradually increases with temperature, as previously reported for AFM studies on similar pNIPAAm-based layers.^[39]

4. Conclusions

A new method for in situ observation of highly swollen hydrogel nanostructures is reported and applied for the investigation of unusual properties of arrays of thermo-responsive hydrogel nanopillars. These structures were prepared from a photo-crosslinkable pNIPAAm-based polymer by nanoimprint lithography. The swelling and collapsing of periodic arrays of imprinted pNIPAAm nanopillars were observed by a combination of diffraction measurements and optical waveguide spectroscopy in comparison to the AFM results. In situ AFM (under water) was capable to capture the topographic features of the nanopillars in direct contact with water only at temperatures above the LCST where the structures were collapsed and sufficiently rigid. However, measurement of the optical waveguide-enhanced diffraction allowed observation of swelling above as well as below LCST. With the aid of an appropriate model the key characteristics could be determined from the optical measurements and these results were found to be fully consistent with the AFM observations. Interestingly, the obtained results indicate that the swelling ratio of nanopillars (allowed to expand and contract in 3D) is similar to that of a tethered thin pNIPAAm hydrogel film (which swells and collapses predominantly in 1D). The temperature-induced collapsing of pNIPAAm leads to the preservation of the nanopillar structure during drying. Bending of these structures was observed when the temperature was raised above the LCST, which is explained by the attractive hydrophobic interaction with the underneath hydrogel surface. The structure can be reversibly erased by drying at temperatures below the LCST and recovered by swelling at temperature below LCST and drying at elevated temperatures above the LCST. The presented approach provides versatile platform for in situ observation of low refractive index contrast nanostructures from materials like highly swollen hydrogels. The investigated thermo-responsive material can find its applications in areas such as sensing (e.g., humidity sensor in food packaging with naked eye readout of diffraction) or security features, which will be subject to following research.

Supporting Information

Supporting Information is available from the Wiley Online Library or from the author.

Acknowledgements: The authors would like to acknowledge the partial support for this work provided by Austrian Science Fund (FWF) through the project ACTIPLAS (P 244920-N20), the International Graduate School BioNanoTech (IGS) Program of the Federal Ministry for Science and Research, Austria, and by the Italian FIRB 2011 NEWTON (RBAP11BYNP). N.S. also acknowledges support from the School of Materials Science and Engineering and the provost's office, Nanyang Technological University, and J.D. received support from Tan Chin Tuan Foundation.

Received: August 22, 2016; Revised: November 16, 2016;
Published online: ; DOI: 10.1002/macp.201600400

Keywords: diffraction; hydrogel; nanoimprint lithography; nanostructure; optical waveguide spectroscopy

- [1] T. R. Hoare, D. S. Kohane, *Polymer* **2008**, *49*, 1993.
- [2] W. Gao, D. Vecchio, J. Li, J. Zhu, Q. Zhang, V. Fu, J. Li, S. Thamphiwatana, D. Lu, L. Zhang, *ACS Nano* **2014**, *8*, 2900.
- [3] L. E. Strong, S. N. Dahotre, J. L. West, *J. Controlled Release* **2014**, *178*, 63.
- [4] S. J. Hollister, *Nat. Mater.* **2005**, *4*, 518.
- [5] M. Thery, V. Racine, A. Pepin, M. Piel, Y. Chen, J. B. Sibarita, M. Bornens, *Nat. Cell Biol.* **2005**, *7*, 947.
- [6] V. L. Alexeev, S. Das, D. N. Finegold, S. A. Asher, *Clin. Chem.* **2004**, *50*, 2353.
- [7] A. K. Geim, S. V. Dubonos, I. V. Grigorieva, K. S. Novoselov, A. A. Zhukov, S. Y. Shapoval, *Nat. Mater.* **2003**, *2*, 461.
- [8] N. J. Glassmaker, T. Himeno, C. Y. Hui, J. Kim, *J. R. Soc. Interface* **2004**, *1*, 23.
- [9] L. Dong, A. K. Agarwal, D. J. Beebe, H. R. Jiang, *Nature* **2006**, *442*, 551.
- [10] J. H. Holtz, S. A. Asher, *Nature* **1997**, *389*, 829.
- [11] J.-H. Kang, J. H. Moon, S.-K. Lee, S.-G. Park, S. G. Jang, S. Yang, S.-M. Yang, *Adv. Mater.* **2008**, *20*, 3061.
- [12] Z. Nie, E. Kumacheva, *Nat. Mater.* **2008**, *7*, 277.
- [13] V. R. Tirumala, R. Divan, L. E. Ocola, D. C. Mancini, *J. Vac. Sci. Technol. B: Microelectron. Nanometer Struct. – Process., Meas., Phenom.* **2005**, *23*, 3124.
- [14] M. Caldorera-Moore, M. K. Kang, Z. Moore, V. Singh, S. V. Sreenivasan, L. Shi, R. Huang, K. Roy, *Soft Matter* **2011**, *7*, 2879.
- [15] F. D. Benedetto, A. Biasco, D. Pisignano, R. Cingolani, *Nanotechnology* **2005**, *16*, S165.
- [16] M. Bae, R. Divan, K. J. Suthar, D. C. Mancini, R. A. Gemeinhart, *J. Vac. Sci. Technol., B: Microelectron. Nanometer Struct. – Process., Meas., Phenom.* **2010**, *28*, C6P24.
- [17] N. Sharma, C. Petri, U. Jonas, J. Dostalek, *Opt. Express* **2016**, *24*, 2457.
- [18] C.-W. Kuo, J.-Y. Shiu, P. Chen, *Chem. Mater.* **2003**, *15*, 2917.
- [19] S. Y. Chou, P. R. Krauss, W. Zhang, L. J. Guo, L. Zhuang, *J. Vac. Sci. Technol., B* **1997**, *15*, 2897.
- [20] D. Ho, J. Zou, B. Zdyrko, K. S. Iyer, I. Luzinov, *Nanoscale* **2015**, *7*, 401.
- [21] E. M. White, J. Yatvin, J. B. Grubbs, J. A. Bilbrey, J. Locklin, *J. Polym. Sci., Part B: Polym. Phys.* **2013**, *51*, 1084.
- [22] J. W. Yoon, S. Q. Cai, Z. G. Suo, R. C. Hayward, *Soft Matter* **2010**, *6*, 6004.
- [23] A. Mateescu, Y. Wang, J. Dostalek, U. Jonas, *Membranes* **2012**, *2*, 40.
- [24] K. A. Melzak, A. Mateescu, J. L. Toca-Herrera, U. Jonas, *Langmuir* **2012**, *28*, 12871.

- [25] X. Dong, X. B. Zou, X. Y. Liu, P. Lu, J. M. Yang, D. L. Lin, L. Zhang, L. S. Zha, *Colloid Surf., A* **2014**, *452*, 46.
- [26] A. Nykänen, M. Nuopponen, P. Hiekkataipale, S. Hirvonen, A. Soininen, H. Tenhu, O. Ikkala, R. Mezzenga, J. Ruokolainen, *Macromolecules* **2008**, *41*, 3243.
- [27] M. E. A. Yoshinobu, *J. Appl. Polym. Sci.* **1994**, *53*, 1203.
- [28] M. Gianneli, P. W. Beines, R. F. Roskamp, K. Koynov, G. Fytas, W. Knoll, *J. Phys. Chem. C* **2007**, *111*, 13205.
- [29] M. A. Plum, W. Steffen, G. Fytas, W. Knoll, B. Menges, *Opt. Express* **2009**, *17*, 10364.
- [30] J. Dostalek, W. Knoll, in *Polymer Science: A Comprehensive Reference* (Eds: K. Matyjaszewski, M. Möller), Elsevier, Amsterdam **2012**, p. 647.
- [31] N. Zhang, W. Knoll, *Anal. Chem.* **2009**, *81*, 2611.
- [32] P. W. Beines, I. Klosterkamp, B. Menges, U. Jonas, W. Knoll, *Langmuir* **2007**, *23*, 2231.
- [33] A. Aulasevich, R. F. Roskamp, U. Jonas, B. Menges, J. Dostalek, W. Knoll, *Macromol. Rapid Commun.* **2009**, *30*, 872.
- [34] A. Mourran, Y. D. Wu, R. A. Gumerov, A. A. Rudov, Igor I. Potemkin II, A. Pich, M. Moller, *Langmuir* **2016**, *32*, 723.
- [35] M. M. Braun, L. Pilon, *Thin Solid Films* **2006**, *496*, 505.
- [36] G. M. Hale, M. R. Query, *Appl. Opt.* **1973**, *12*, 555.
- [37] R. Toomey, D. Freidank, J. Ruhe, *Macromolecules* **2004**, *37*, 882.
- [38] M. Guvendiren, S. Yang, J. A. Burdick, *Adv. Funct. Mater.* **2009**, *19*, 3038.
- [39] M. J. N. Junk, R. Berger, U. Jonas, *Langmuir* **2010**, *26*, 7262.